

Electronic structure of nitrogen-vacancy doped SmN: Intermediate valence and 4*f* transport in a ferromagnetic semiconductor

W. F. Holmes-Hewett 

The MacDiarmid Institute for Advanced Materials and Nanotechnology and The School of Chemical and Physical Sciences, Victoria University of Wellington, P.O. Box 600, Wellington 6140, New Zealand



(Received 15 July 2021; accepted 3 August 2021; published 16 August 2021)

SmN is an intrinsic ferromagnetic semiconductor with electrical transport properties that have been of recent experimental interest. Its conductivity is largely dictated by the concentration of nitrogen vacancies that dope the crystal with electrons. Here, we present a density functional theory based study of SmN, variously doped with nitrogen vacancies. We find that the Sm ions which coordinate a nitrogen vacancy take on an intermediate 2–3⁺ valence, while the remaining Sm ions in the crystal remain trivalent. Our results show that the localized 4*f* states hybridize with the extended state Sm 5*d* and N 2*p* bands and are involved in electron transport throughout the crystal.

DOI: [10.1103/PhysRevB.104.075124](https://doi.org/10.1103/PhysRevB.104.075124)

I. INTRODUCTION

The hybridization of localized and extended states at the Fermi energy of a material gives rise to some of the most enigmatic behaviors currently known to condensed matter physics [1–6]. Lanthanide compounds have led as examples of this correlated behavior, and although the rare earth mononitrides (LN, L a lanthanide) were proposed already as likely correlated electron materials [7,8], that prediction has not yet been explored. Here, we discuss in this context a computational investigation of one member of the series, SmN.

The LN form in the simple rocksalt structure with L³⁺ and N³⁻ ions, shown in Fig. 1. The combination and competition of spin and orbital moments in the L 4*f* electron shell give rise to a wide range of magnetic behaviors [9]. Although most have a ferromagnetic ground state, the saturation moments and coercive fields vary by orders of magnitude throughout the series. The nonmagnetic end members of the series LaN and LuN have completely empty and filled 4*f* shells, respectively, with these empty states lying far above and the filled states far below the Fermi energy. The transport properties of these materials are dominated by the L 5*d* conduction band.

The central member of the series GdN has a half-filled 4*f* shell, now with a ferromagnetic ground state. The seven filled majority spin 4*f* states are ~7 eV below the Fermi energy and the seven unfilled minority spin 4*f* states ~5 eV above [10–12]. The 4*f* states in GdN play only an indirect role in the transport properties. The ferromagnetic 4*f*/5*d* and antiferromagnetic 5*d*/N 2*p* exchange results in majority spin charge carriers in both the valence band maximum and conduction band minimum. The remaining LN have more complex transport properties with filled/unfilled 4*f* bands treading though and hybridizing with the conduction and valence bands. The LN are poised at a metal-insulator boundary. In the stoichiometric state the LN are insulating, however, they can be doped with electrons via nitrogen vacancies.

Density functional theory (DFT) calculations have been completed for the entire series [11], however only a single calculation exists for a nitrogen-vacancy doped LN, GdN [13]. This calculation finds all that the Gd ions remain trivalent, as in the stoichiometric crystal. There are thus three electrons released by the vacancy, two of which are weakly bound to the vacancy site. The third lifts the Fermi energy into a hybridized impurity-state/Gd 5*d* conduction band. The picture is then of an extended state metallic material, which is consistent with recent experimental results on heavily doped GdN thin films [14]. Studies on the other LN are mostly on nominally undoped to moderately doped thin films and they are in general consistent with the existing calculations on stoichiometric crystals. There are clear signatures of a narrow band gap [15–21] and a dopable semiconducting ground state, which is controlled by a residual concentration of nitrogen vacancies [13,22–24].

The trivalent Sm in stoichiometric SmN has the configuration ⁶H_{5/2} [25,26]. It is ferromagnetic below 30 K with a near-zero saturation magnetization of 0.035μ_B per Sm³⁺. The vanishingly small moment represents a near balance between opposing spin and orbital contributions [26–28]. The conduction and valence bands, as with the other LN, are dominated by the extended state L 5*d* and N 2*p* bands, respectively. The insulating nature of the undoped ferromagnetic films implies that the two unfilled majority spin 4*f* bands are above the Fermi energy, while the five filled bands are below. This is reflected in band structure calculations on stoichiometric SmN, which place the unfilled majority spin 4*f* bands ~1 eV above the Sm 5*d* conduction band minimum [11]. However, the direct influence of these 4*f* bands on the transport properties of SmN has been seen in experiment [29], including the observation of unconventional superconductivity [30] in moderately doped films. Furthermore, optical spectroscopy measurements have found evidence of 4*f* states near the base of the conduction band [20]. Reconciling these experimental

results with the existing band structure calculations on stoichiometric SmN remains problematic.

In the present paper we present a computational study of SmN variously doped with nitrogen vacancies, at concentrations which reflect the experimental literature. Band structure calculations find that stoichiometric SmN has an insulating ground state, while nitrogen-vacancy doped SmN has a finite density of states at the Fermi energy. These results, however, strongly contrast those of nitrogen-vacancy doped GdN [13]. In SmN we find that rather than raising the Fermi energy into the $5d$ extended states, the $4f$ bands on the six nearest-neighbor Sm ions become partially occupied, and fall into the intrinsic band-gap region. This results in an intermediate $2-3^+$ valence for these six ions, while the remaining Sm ions in the crystal remain trivalent. These results are consistent with recent experimental reports and provide insight into the electrical transport properties of SmN. They also highlight the role of the $4f$ states in the LN, and show that for many of the series these bands may contribute much more than simply dictating the magnetic properties of the material.

II. COMPUTATIONAL DETAILS

Calculations were undertaken using QUANTUM ESPRESSO [31,32] and the rare earth pseudopotentials developed by Topskál *et al.* [33]. For the primitive cell calculations the Brillouin zone was sampled with a grid of $12 \times 12 \times 12$ k points, and supercell calculations were sampled on a $4 \times 4 \times 4$ grid. The wave function and charge density cutoff energies were 50 and 200 Ry, respectively, for all calculations. Gaussian broadening has been applied to the density of states calculations.

The $4f$ electrons of the LN series are strongly correlated and thus require careful treatment beyond the local spin density (LSDA), or generalized gradient (GGA) approximation [10,11]. In the basic LSDA/GGA the $4f$ states would be found at the Fermi energy for most of the LN. In reality the strongly correlated nature of these electrons pushes the filled states below and unfilled states above the Fermi energy. This physics can be captured using the DFT+ U method [34–37]. In the present study two U parameters are used, as described in Refs. [10,11,15]. U_f accounts for the strongly correlated $4f$ states, and U_d is applied to the $5d$ states and used to match the optical band gap to the experimental value. Double counting is accounted for in the fully localized limit.

To begin, band structure calculations of stoichiometric SmN were undertaken. This required determining the two terms, U_f and U_d . The first of these, U_f , was calculated from first principles [38] in a self-consistent manner. U_f was first calculated at the equilibrium lattice parameter, the lattice was then re-relaxed and U_f calculated again, and this was repeated until a stable solution was found. Once U_f was found U_d was estimated by matching the calculated optical band gap to the experimental data [20,39]; this was also completed in a self-consistent manner with the lattice re-relaxed at each stage. Calculations for nitrogen-vacancy doped SmN were conducted using the U_f and U_d parameters found for the undoped cell.

Three different vacancy concentrations were investigated, including the undoped cell. The calculations for the 3% and 5% vacancy concentrations were run on supercells of $3 \times 3 \times$

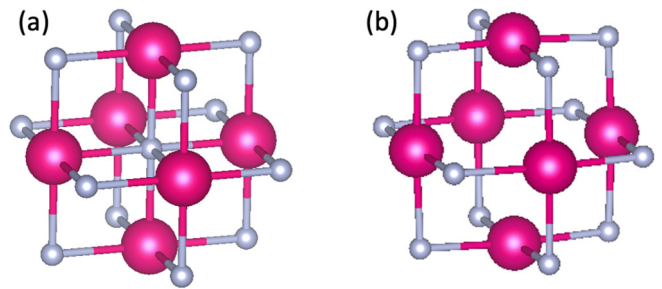


FIG. 1. (a) The rocksalt structure of stoichiometric SmN. (b) A nitrogen vacancy creates a structural distortion, with all the surrounding ions pulled outwards. The six nearest-neighbor and 12 next-nearest-neighbor ions are shown.

3 and $2 \times 3 \times 3$ primitive unit cells, respectively, with each containing a single nitrogen vacancy. These concentrations are comparable with moderately to heavily doped SmN films in the experimental literature [24,29,30]. The supercells were fully relaxed to accommodate the vacancy, and the band structures were unfolded so they can be easily compared to the band structures of the primitive unit cell. For details of the unfolding procedure, please see Ref. [40].

III. RESULTS

A. Stoichiometric SmN

The electronic structure calculations for stoichiometric SmN are shown in Figs. 2(a)–2(c). To begin we discuss the Sm $4f$ bands, which can be identified most easily as corresponding to the red series in the density of states plot [Fig. 2(b)]. The position of these is largely determined by U_f , which we calculate as $U_f = 6.76$ eV. The five filled majority spin $4f$ bands are ~ 6 eV below the valence band maximum (not shown). The two unfilled majority spin $4f$ bands thread through and hybridize with the Sm $5d$ bands roughly 1 eV above the conduction band minimum. The unfilled minority spin $4f$ bands are found in two groups ~ 3.5 and 4.5 eV above the conduction band minimum.

The calculation finds an optical gap at the X point of ~ 0.6 eV. As described previously, the optical gap has been adjusted by applying U_d to the Sm $5d$ bands, which we find as $U_d = 4.3$ eV. For SmN, low temperature optical measurements are not available; thus we match the average energy of the majority and minority spin bands at X to the measured optical gap in the paramagnetic phase [20,39]. Significantly, our calculations result in an indirect Γ - X gap of ~ 0.15 eV, making the material insulating in the ground state, which is supported by the majority of recent experimental studies [9,20,24–27,29,30]. The Gaussian broadening applied to the density of states in Fig. 2(b) obscures the small indirect gap.

B. Doped supercells

Before the electronic structure was calculated the atomic positions and volume of the supercell were allowed to fully relax to accommodate the nitrogen vacancy. The final cell volumes of the doped cells were 3% and 3.6% larger than the

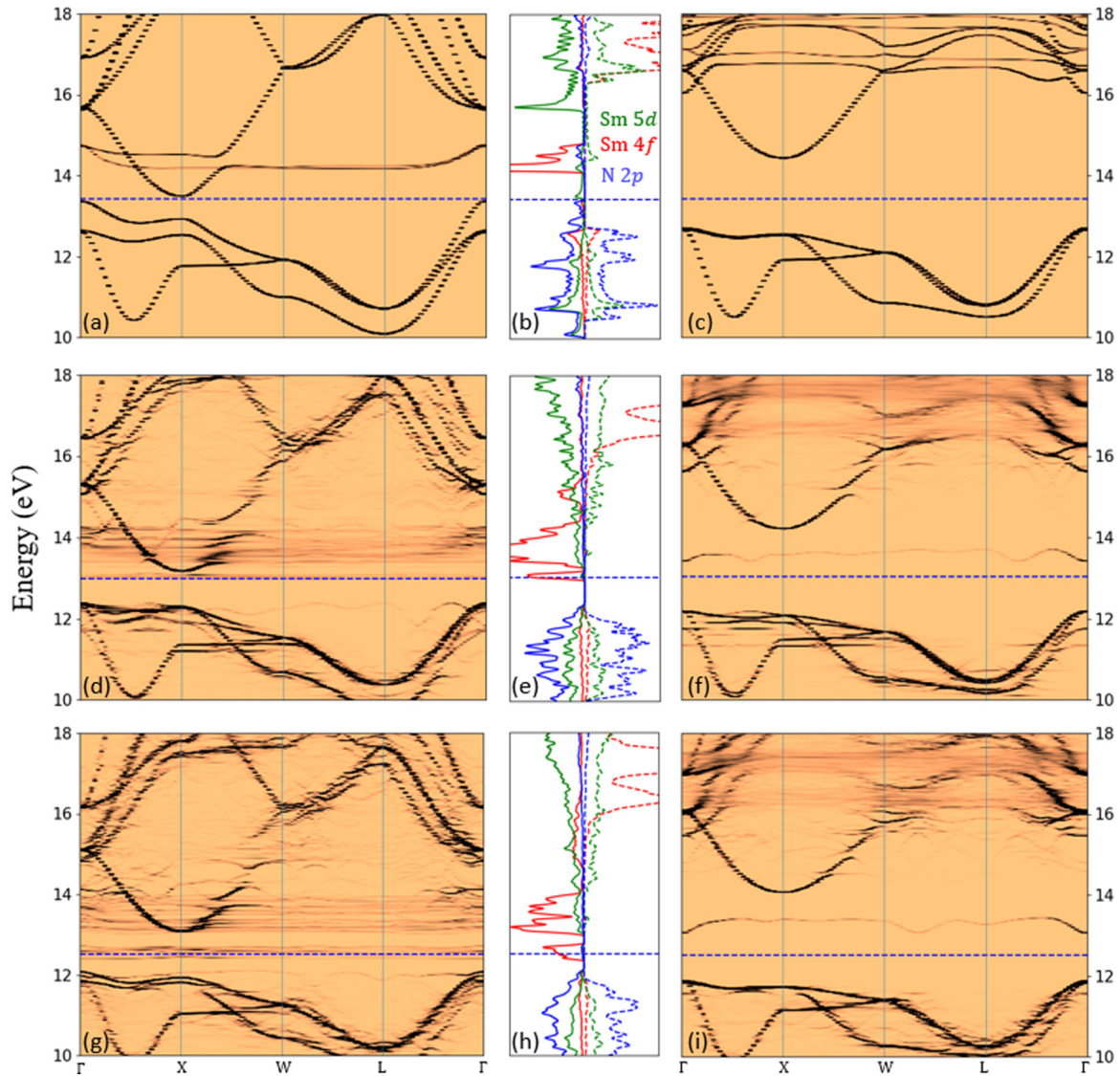


FIG. 2. (a)–(c) Stoichiometric SmN: (a) Majority spin bands. (b) Density of states (majority spin: left solid, and minority spin: right dashed). (c) Minority spin bands. (d)–(f) 3% nitrogen-vacancy doped SmN: (d) Majority spin bands. (e) Density of states. (f) Minority spin bands. (g)–(i) 5% nitrogen-vacancy doped SmN: (g) Majority spin bands. (h) Density of states. (i) Minority spin bands. The Fermi energy is shown as the blue dashed line in all plots.

volume of the undoped cell for the 3% and 5% doped cells, respectively. Figure 1(a) shows the stoichiometric structure and Fig. 1(b) shows the structure immediately surrounding the vacancy site of the 3% doped supercell. In the undoped cell the central N ion represents a negative charge, which is largely missing in the doped supercell. The lack of this central negative charge causes the six Sm ions which coordinate the vacancy to be pulled away from the vacancy site by the surrounding N ions. The distance between a nearest-neighbor Sm ion and the center of the vacancy site is extended by $\sim 3\%$ compared to the distance between a Sm ion and N ion in the undoped cell. This behavior, relaxing away from the vacancy site, is similar to what was found computationally for nitrogen-vacancy doped GdN [13]. Interestingly both these computational studies oppose the conclusions of an experimental study on GdN [41], and results on some other nitride compounds [42,43].

The unfolded supercell band structure calculations for the 3% doped cell are shown in Figs. 2(d)–2(f). The plots show substantial disorder caused by both structural and charge inhomogeneity throughout the supercell. The periodic nature of the calculation means these deformations introduce new long-range periodicities into the crystal and thus new states. The dispersion in many of these states would not be well defined in the physical material, which has a random array of vacancies. The disorder and additional states make interpreting the bands somewhat problematic. The density of states, being a quantity which is integrated over the entire Brillouin zone, does not suffer the same issues. In any case, the supercell band structures shown in Figs. 2(d) and 2(f) show many similar features to the calculations on the stoichiometric material. The Sm 5d band once again has a minimum at X rising towards Γ and W. The N 2p valence band still finds a maximum at Γ , however, the drop towards X is much less significant than in

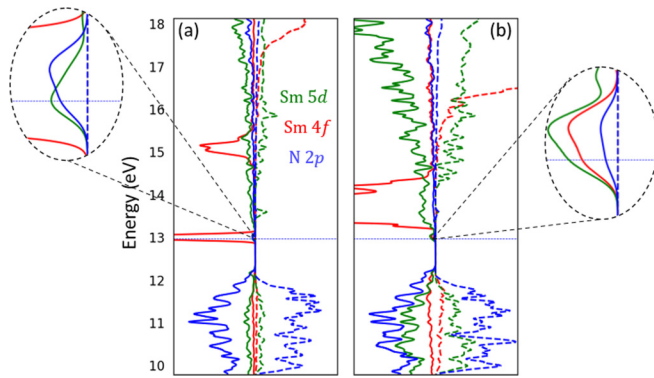


FIG. 3. (a) Density of states for the six Sm nearest neighbors and 12 N next-nearest neighbors to the vacancy. (b) Density of states for the remaining ions in the cell. Both plots refer to the 3% doped supercell. The Fermi energy is shown as the blue dashed line in both plots.

the stoichiometric case. The spin splitting in the valence band is significantly reduced.

The Sm $4f$ states in the doped supercell are significantly different from those in the stoichiometric material. These states have become even more atomiclike, with the majority spin $4f$ bands of the stoichiometric material splitting into two disconnected groups, which are most easily identified in the density of states shown in Fig. 2(e). One of the groups spans the base of the Sm $5d$ bands to roughly 1 eV higher, while the other straddles the Fermi energy in the intrinsic band-gap region near 13 eV. The Sm $4f$ states are discussed in more detail below.

Near the top of the majority spin valence band in Fig. 2(d) there is a band which spans the zone. This state appears to be localized, given the lack of curvature, and is very similar to the states noted in nitrogen-vacancy doped GdN [13] and found to be bound to the vacancy site. A similar localized state can be seen in the minority spin bands in Fig. 2(f) at ~ 13.5 eV, but in this case it is unfilled.

Figures 2(g)–2(i) show the band structure of a 5% doped cell. Once again the Sm $4f$ bands have split into two groups, one of which covers the lower portion of the Sm $5d$ bands, while the other is in the intrinsic band-gap region, again straddling the Fermi energy.

Returning to the discussion of the $4f$ states in the 3% doped supercell, the two groups of Sm $4f$ states, discussed above from Fig. 2(e), can be separated by observing the density of states for different regions of the crystal, revealing a clear charge inhomogeneity for the Sm ions. Figure 3(a) shows the density of states for the six nearest-neighbor Sm ions and 12 next-nearest-neighbor N ions, which collectively coordinate the nitrogen vacancy (as seen in Fig. 1). Figure 3(b) shows the density of states of the remaining ions in the crystal. Here, we see that the majority spin $4f$ states on the Sm ions which coordinate the vacancy form the group of $4f$ states which straddle the Fermi energy. The majority spin $4f$ states on these Sm ions are partially filled. Integrating the density of states corresponding to these partially filled $4f$ states shows ~ 1 electron is shared by these six ions, which thus have an intermediate $2\text{--}3^+$ valence. Figure 3(b) shows that the $4f$

states on the remaining ions in the crystal remain largely above the Fermi energy; these ions retain the 3^+ valence of the stoichiometric crystal.

The elliptical zooms on each panel show the density of states at the Fermi energy. It is important to note that this is nonzero throughout the crystal. The Sm $4f$, $5d$ and N $2p$ wave functions each have weight at the Fermi energy in both plots. There is some degree of coupling between the $4f$ states on the Sm ions coordinating the vacancy and elsewhere in the crystal, which looks to be mediated via hybridization with the $5d$ and N $2p$ bands, thus facilitating electrical transport. The three electrons, which in the stoichiometric case would have been found on the N ion at the vacancy site, are not entirely contained by the 18 nearest/next-nearest-neighbor ions to the vacancy. It appears that roughly one of the electrons is shared by the $4f$ states on the six Sm ions coordinating the vacancy. The other two electrons are released into the valence band and represented by the filled impurity states and hybridized states discussed above.

The present calculations, when compared to similar calculations on GdN [13], show SmN reacts very differently to the inclusion of a nitrogen vacancy. Rather than raising the Fermi energy into the Sm $5d$ bands throughout the crystal, the three electrons related to the vacancy are largely localized to the region surrounding the vacancy, and result in an intermediate valence for the nearest-neighbor Sm ions. It is certain that the electronic environment local to the Sm ions which coordinate the vacancy is significantly different from those in undoped regions of the crystal, and strongly affects the $4f$ states on these ions. The calculations are consistent with experimental studies which have concluded the $4f$ band has influence over the transport properties in SmN [20,29]. Of particular interest is the observation of superconductivity in SmN [30], which was understood in terms of transport in a mixed $4f/5d$ band, with the present results implying this transport scenario is precisely the case.

These calculations furthermore imply SmN may be a useful material in which to search for electron correlation effects, which generally manifest when there exists a hybridization between extended and localized states at the Fermi energy. Figure 3 implies this is the case in SmN, and furthermore the involvement of the extended/localized states can likely be tuned by vacancy doping. These calculations highlight the influence of the $4f$ states on the transport properties of SmN, and show that for many of the LN the $4f$ states contribute much more than simply dictating the magnetic behavior.

IV. CONCLUSIONS

Calculations on stoichiometric SmN, which have been adjusted to reproduce the measured optical band gap, result in an insulating ground state in agreement with the majority of the experimental literature. When the crystal is doped with nitrogen vacancies the six Sm ions which coordinate the vacancy house roughly one of the three electrons released, resulting in an intermediate valence for these ions. The other electrons relating to the vacancy are released into the valence band. The Sm $4f$ states on the six nearest-neighbor ions fall to the Fermi energy and weakly hybridize with the N $2p$ and Sm $5d$ wave functions throughout the crystal. The present calculations

strongly contrast similar calculations on GdN and highlight the importance of the $4f$ states in not only the magnetic but also the electrical transport properties of the LN. They are consistent with experimental reports which imply $4f$ weight in the transport channel and highlight SmN as a candidate for the investigation of correlated electron behaviors.

ACKNOWLEDGMENTS

I wish to acknowledge my colleagues with whom I have engaged in robust discussions on the present material,

particularly J. Trodahl, B. Ruck, and B. Buckley. The computations were performed on the Rāpoi high performance computing facility of Victoria University of Wellington and New Zealand eScience Infrastructure (NeSI) high performance computing facility. New Zealand's national facilities are provided by NeSI and funded jointly by NeSI's collaborator institutions and through the Ministry of Business, Innovation and Employment's Research Infrastructure programme [44]. This research was supported by the New Zealand Endeavour Fund (Grant No. RTVU1810). The MacDiarmid Institute is supported under the New Zealand Centres of Research Excellence Programme.

-
- [1] S. Wirth and F. Steglich, *Nat. Rev. Mater.* **1**, 16051 (2016).
- [2] D. N. Basov, R. D. Averitt, D. van der Marel, M. Dressel, and K. Haule, *Rev. Mod. Phys.* **83**, 471 (2011).
- [3] P. Coleman, in *Handbook of Magnetism and Advanced Magnetic Materials*, edited by J. H. Kronmüller, S. Parkin, M. Fähnle, S. Maekawa, and I. Zutic (American Cancer Society, Hoboken, NJ, 2007).
- [4] R. Adler, C.-J. Kang, C.-H. Yee, and G. Kotliar, *Rep. Prog. Phys.* **82**, 012504 (2018).
- [5] L. Taillefer, *Annu. Rev. Condens. Matter Phys.* **1**, 51 (2010).
- [6] M. Dzero, J. Xia, V. Galitski, and P. Coleman, *Annu. Rev. Condens. Matter Phys.* **7**, 249 (2016).
- [7] L. Petit, R. Tyer, Z. Szotek, W. M. Temmerman, and A. Svane, *New J. Phys.* **12**, 113041 (2010).
- [8] L. Petit, Z. Szotek, M. Lüders, and A. Svane, *J. Phys.: Condens. Matter* **28**, 223001 (2016).
- [9] F. Natali, B. J. Ruck, N. O. V. Plank, H. J. Trodahl, S. Granville, C. Meyer, and W. R. L. Lambrecht, *Prog. Mater. Sci.* **58**, 1316 (2013).
- [10] P. Larson and W. R. L. Lambrecht, *Phys. Rev. B* **74**, 085108 (2006).
- [11] P. Larson, W. R. L. Lambrecht, A. Chantis, and M. van Schilfgaarde, *Phys. Rev. B* **75**, 045114 (2007).
- [12] Z. C. Gernhart, J. A. Colón Santana, L. Wang, W.-N. Mei, and C. L. Cheung, *MRS Proc.* **1729**, 131 (2015).
- [13] A. Punya, T. Cheiwchanhangngij, A. Thiess, and W. R. L. Lambrecht, *MRS Proc.* **1290**, 4 (2011).
- [14] T. Maity, H. J. Trodahl, F. Natali, B. J. Ruck, and S. Vézian, *Phys. Rev. Materials* **2**, 014405 (2018).
- [15] H. J. Trodahl, A. R. H. Preston, J. Zhong, B. J. Ruck, N. M. Strickland, C. Mitra, and W. R. L. Lambrecht, *Phys. Rev. B* **76**, 085211 (2007).
- [16] C. Mitra and W. R. L. Lambrecht, *Phys. Rev. B* **78**, 195203 (2008).
- [17] H. Yoshitomi, S. Kitayama, T. Kita, O. Wada, M. Fujisawa, H. Ohta, and T. Sakurai, *Phys. Rev. B* **83**, 155202 (2011).
- [18] R. Vidyasagar, S. Kitayama, H. Yoshitomi, T. Kita, T. Sakurai, and H. Ohta, *Appl. Phys. Lett.* **100**, 232410 (2012).
- [19] R. Vidyasagar, T. Kita, T. Sakurai, and H. Ohta, *J. Appl. Phys.* **115**, 203717 (2014).
- [20] W. F. Holmes-Hewett, R. G. Buckley, B. J. Ruck, F. Natali, and H. J. Trodahl, *Phys. Rev. B* **99**, 205131 (2019).
- [21] W. F. Holmes-Hewett, R. G. Buckley, B. J. Ruck, F. Natali, and H. J. Trodahl, *Phys. Rev. B* **100**, 195119 (2019).
- [22] N. O. V. Plank, F. Natali, J. Galipaud, J. H. Richter, M. Simpson, H. J. Trodahl, and B. J. Ruck, *Appl. Phys. Lett.* **98**, 112503 (2011).
- [23] W. F. Holmes-Hewett, C. Pot, R. G. Buckley, A. Koo, B. J. Ruck, F. Natali, A. Shaib, J. D. Miller, and H. J. Trodahl, *Appl. Phys. Lett.* **117**, 222409 (2020).
- [24] A. Shaib, W. F. Holmes-Hewett, J. Chan, P. P. Murmu, B. J. Ruck, H. J. Trodahl, and F. Natali, *AIP Advances* **11**, 015125 (2021).
- [25] A. R. H. Preston, S. Granville, D. H. Housden, B. Ludbrook, B. J. Ruck, H. J. Trodahl, A. Bittar, G. V. M. Williams, J. E. Downes, A. DeMasi, Y. Zhang, K. E. Smith, and W. R. L. Lambrecht, *Phys. Rev. B* **76**, 245120 (2007).
- [26] E.-M. Anton, B. J. Ruck, C. Meyer, F. Natali, H. Warring, F. Wilhelm, A. Rogalev, V. N. Antonov, and H. J. Trodahl, *Phys. Rev. B* **87**, 134414 (2013).
- [27] C. Meyer, B. J. Ruck, J. Zhong, S. Granville, A. R. H. Preston, G. V. M. Williams, and H. J. Trodahl, *Phys. Rev. B* **78**, 174406 (2008).
- [28] J. F. McNulty, B. J. Ruck, and H. J. Trodahl, *Phys. Rev. B* **93**, 054413 (2016).
- [29] W. F. Holmes-Hewett, F. H. Ullstad, B. J. Ruck, F. Natali, and H. J. Trodahl, *Phys. Rev. B* **98**, 235201 (2018).
- [30] E.-M. Anton, S. Granville, A. Engel, S. V. Chong, M. Governale, U. Zülicke, A. G. Moghaddam, H. J. Trodahl, F. Natali, S. Vézian, and B. J. Ruck, *Phys. Rev. B* **94**, 024106 (2016).
- [31] P. Giannozzi, S. Baroni, N. Bonini, M. Calandra, R. Car, C. Cavazzoni, D. Ceresoli, G. L. Chiarotti, M. Cococcioni, I. Dabo *et al.*, *J. Phys.: Condens. Matter* **21**, 395502 (2009).
- [32] P. Giannozzi, O. Andreussi, T. Brumme, O. Bunau, M. B. Nardelli, M. Calandra, R. Car, C. Cavazzoni, D. Ceresoli, M. Cococcioni *et al.*, *J. Phys.: Condens. Matter* **29**, 465901 (2017).
- [33] M. Topsakal and R. Wentzcovitch, *Comput. Mater. Sci.* **95**, 263 (2014).
- [34] V. I. Anisimov, J. Zaanen, and O. K. Andersen, *Phys. Rev. B* **44**, 943 (1991).
- [35] V. I. Anisimov, I. V. Solovyev, M. A. Korotin, M. T. Czyżyk, and G. A. Sawatzky, *Phys. Rev. B* **48**, 16929 (1993).
- [36] A. I. Liechtenstein, V. I. Anisimov, and J. Zaanen, *Phys. Rev. B* **52**, R5467(R) (1995).

- [37] M. Cococcioni and S. de Gironcoli, *Phys. Rev. B* **71**, 035105 (2005).
- [38] I. Timrov, N. Marzari, and M. Cococcioni, *Phys. Rev. B* **98**, 085127 (2018).
- [39] M. Azeem, *Chin. J. Phys.* **56**, 1925 (2018).
- [40] V. Popescu and A. Zunger, *Phys. Rev. B* **85**, 085201 (2012).
- [41] K. Senapati, T. Fix, M. E. Vickers, M. G. Blamire, and Z. H. Barber, *Phys. Rev. B* **83**, 014403 (2011).
- [42] L. Skala and P. Capkova, *J. Phys.: Condens. Matter* **2**, 8293 (1990).
- [43] R. Kaufmann and O. Meyer, *Solid State Commun.* **51**, 539 (1984).
- [44] <https://www.nesi.org.nz>.